Predictive Modeling of the Softness of Facial Tissue Products: A Spectral Analysis Approach

Yong Ju Lee 🗓, Ji Eun Cha, Geon-Woo Kim, Tai-Ju Lee,* and Hyoung Jin Kim 🧓,*

Softness is a critical yet subjective characteristic of hygiene paper products such as facial tissues. In this study, softness values were obtained from the authors' previous research using the Interval Scale Value (ISV) method, involving panelists' round-robin pairwise comparisons. A machine-learning approach was developed to predict softness from one-dimensional power spectral density (1D-PSD) spectra of surface roughness profiles. Using seven commercial samples and an optimized multilayer perceptron model, a achieved high predictive performance ($R^2 = 0.860$) was achieved without additional measurements such as tensile modulus or surface friction. This work highlights the potential of combining spectral analysis and machine learning for objective softness evaluation.

DOI: 10.15376/biores.20.3.6457-6475

Keywords: Surface roughness; Fast Fourier transform (FFT); Power spectral density (PSD); Sensory panel test (SPT); Multilayer perceptron (MLP)

Contact information: Department of Forest Products and Biotechnology, Kookmin University, 77 Jeongneung-ro, Seongbuk-gu, Seoul 02707 Republic of Korea;

* Corresponding authors: hyjikim@kookmin.ac.kr; leetj@kookmin.ac.kr

INTRODUCTION

Softness is regarded as a crucial characteristic of paper products for hygiene, such as bathroom and facial tissues. Softness, being inherently subjective, has often been considered difficult to assess through objective testing methods. However, ongoing efforts to develop such methods persist, given their significant advantages when successfully implemented. Subjective methods, by contrast, are retrospective in nature and may not provide the proactive insights needed for tissue manufacturers to innovate effectively (Ko et al. 2017).

Given their subjectiveness, softness attributes have been generally believed to be impossible to evaluate using objective softness test methods. Despite such challenges, there has been a persistent drive to create testing methods, valued for their advantages such as cost efficiency, time saving (e.g., faster time to market), improved quality and process control, and valuable insights and direction for product development (Ko et al. 2015, 2016; Lee et al. 2017, 2023; Kweon et al. 2024).

Building on the pioneering work of Hollmark (1983) and Hollmark and Ampulski (2004), significant progress has been achieved in developing physical softness models for hygiene paper products. Ramasubramanian (2001) also provided a comprehensive review of this topic. Subjective softness primarily comprises two main components: bulk softness and surface softness (Ampulski *et al.* 1991; Beuther *et al.* 2012; Ko *et al.* 2018). For bulk softness measurements, the tensile modulus (*TM*) has been defined as the slope between two specific points on a load–elongation curve (Ko *et al.* 2015). Meanwhile, surface

softness has been assessed using a surface profilometer to measure surface roughness and friction (Ko *et al.* 2015, 2017, 2018).

Lee *et al.* (2023) proposed predictive models for evaluating the softness of facial tissue products. The 3-P geometric mean (GM) model for facial tissue products was identified, which integrated TM, surface roughness, and surface friction. These models were normalized to quantify the contributions of bulk and surface softness. The analysis revealed that surface roughness contributed \sim 50% to the overall softness, with surface friction and TM accounting for 20% and 30%, respectively. Overall, the major component of softness for facial tissue products was surface roughness.

The surface roughness of paper products spans multiple scales, including the microscale (e.g., individual fibers), the intermediate scale (such as creping), and the macroscale, which reflects post-converting processes like printing and embossing (Kajanto et al. 1998; Lee et al. 2023). For the tissue paper products which physical and mechanical properties are dependent on creping and embossing process (Pawlak et al. 2022). Thus, it can be hypothesized that the dominant contributor to the surface roughness of facial tissue products is the macroscale roughness.

Advancements in mathematical algorithms have facilitated the expansion of predictive modeling techniques as alternatives to conventional chemical analysis for characterizing various materials, including pulp and paper products (Kim *et al.* 2023; Hwang *et al.* 2024). Moreover, in the context of physical analyses such as surface characterization, predictive models have demonstrated notable potential and superior performance (Boidi *et al.* 2020; Hasan and Karabacak 2023; Motamedi *et al.* 2023). In this respect, Aguilar *et al.* (2009) employed the friction noise generated by a small brush sliding over the surface of a paper to assess surface roughness. The recorded noise was analyzed using a signal-processing algorithm based on the frequency domain. This approach, combined with an artificial neural network model, enabled the measurement of surface roughness in tissue papers.

This study aims to develop a machine-learning-based technique for measuring the softness of facial tissue products. To this end, a method is proposed to treat random roughness profiles of tissue as distinct features using spectral analysis. This article introduces a novel approach to surface characterization and softness measurement, emphasizing cost-effectiveness and rapid analysis.

EXPERIMENTAL

Materials

The physical properties of seven commercial two-ply facial tissue samples and their interval scale value (ISV) of softness are presented in Table 1. Thurstone (1994) introduced the ISV, which is derived through pair-comparison testing. The ISV plays a critical role in developing physical models for predicting subjective evaluations. Unlike ranking or rating scales, which are neither linear nor continuous on equal intervals (Ko *et al.* 2018; Lee *et al.* 2017), the ISV provides a linear and continuous scale with equal intervals, similar to physical measurements such as length or weight. Statistically, the ISV corresponds to the Z-value of normal deviates and functions similarly to a physical measurement.

In brief, the ISV softness can be determined by a subgrouping approach known as the Ko-method (Ko et al. 2017). In this method, the full sample set is divided into

overlapping subgroups linked by anchor samples, thereby significantly reducing the number of pairwise comparisons required. For example, for seven samples, the full roundrobin pair-comparison would require 21 comparisons; however, using the Ko-method, subgroup one may include samples 1 to 4, and subgroup two samples 4 to 7, with sample 4 serving as the anchor. Additionally, the Ko-method improves data reliability by avoiding pairings with preference values below 20% or above 80%, which addresses the sensitivity of ISV to extreme preference values.

ISV softness and predicted ISV softness were investigated in previous work (Lee et al. 2023). The ISV softness for the seven facial tissue samples was obtained using the aforementioned subgrouping pair-comparison method. Before dividing the samples into two subgroups, a ranking procedure was conducted to identify the anchor sample, with FT4 being selected as it ranked centrally among the samples. Following subgrouping, pairwise comparisons were conducted by 100 untrained panelists (Ko et al. 2016; 2017; 2018; Lee et al. 2017; Lee et al. 2023). The predicted ISV softness of the facial tissue was derived from GM models.

FT8 and FT9, which did not evaluate the ISV softness, were used to predict the ISV softness using the machine-learning-based softness prediction model.

Table 1. Physical Properties of Facial Tissues and ISV Softness (Y. J. Lee et al.
2023)

Sample	Basis Weight (g/m²)	Thickness (mm)	Density (g/cm³)	ISV Softness	Predicted ISV Softness from 3-P Models (TM, RMAD, and FMAD)	Predicted ISV Softness from 2-P Models (TM and RMAD)
FT1	22.9	0.077	0.30	1.69	1.53	1.32
FT2	20.5	0.076	0.27	0.53	0.35	0.48
FT3	14.7	0.046	0.32	0.64	0.36	0.00
FT4	15.6	0.063	0.25	0.53	0.85	0.76
FT5	13.7	0.051	0.27	0.15	0.00	0.19
FT6	12.9	0.055	0.23	0.23	0.48	0.17
FT7	13.6	0.053	0.26	0.00	0.27	0.31
FT8	13.9	0.050	0.27	_	_	_
FT9	15.4	0.066	0.23	_	_	_

Surface Roughness Testing

The samples were conditioned for longer than 48 h at a temperature of $23 \pm 1^{\circ}$ C and a relative humidity (RH) of $50\% \pm 2\%$, according to ISO standard 187, before surface roughness testing.

For the surface roughness testing, a Kawabata surface tester (Model: KES-SESRU, Kato Tech, Kyoto, Japan) was used. Generally, for the surface characterization of tissue paper products, a U-tube stylus is used. However, an excessively large contact area of the stylus is unsuitable for spectral analysis (Wu 2000). To solve this issue, 1.0R conical-shaped styluses were tested (Park *et al.* 2021; Moon *et al.* 2022; Lee *et al.* 2023). These styluses maintain minimal contact with the sample surface because their contact area is small and approximately circular in shape.

The testing conditions were as follows: scan length, 20 mm; scan speed, 1 mm/s; and data acquisition rate, 1000 Hz (or 1000 points/s). For each sample, 10 measurements

were taken in the machine direction. The testing was performed at 23 ± 1 °C and at an RH of 50 ± 2 %. These conditions were successfully applied to the surface characterization of tissue products (Lee *et al.* 2023). Consequently, the surface roughness profile shown in Fig. 1a was obtained.

Determination of the Surface Roughness of Facial Tissues

From the surface roughness profile in Fig. 1a, the average of the surface roughness (R_a) and the mean absolute deviation (RMAD) from R_a were calculated using Eqs. 1 and 2,

$$R_a = \frac{1}{N} \sum_{i=1}^{N} |R_i| \tag{1}$$

$$RMAD = \frac{1}{N} \sum_{1}^{N} \left| |R_i| - R_a \right| \tag{2}$$

where R_a is the roughness average (μ m), R_i is the roughness (μ m) at scanning point i, and N is the number of data points in the scan length.

Power Spectral Density of Surface Roughness Profile

Detrending

Detrending raw data involves removing low-order polynomial terms from the profile to reduce the high-frequency artifacts introduced into the power spectral density (PSD) by endpoint discontinuities. Surface profiles with substantial tilt or curvature must be flattened or "pre-whitened" by eliminating these low-order polynomial components (Blackman and Tukey 1959). Detrending is commonly applied in fast Fourier transform (FFT) processing (Borchers 2022) and can be accomplished by removing the mean value or a (piecewise) linear trend from a vector or from each column of a matrix. The mathematical expression for this process is defined in Eq. 3.

$$\bar{Z}(x_n) = Z(x_n) - [a + bx_n + cx_n^2 + \cdots]$$
 (3)

where $Z(x_n)$ represents the raw data, and the coefficients are computed using a simple least-squares fit to the data points. In this study, surface roughness profiles were detrended by computing the least-squares fit of a straight line (or a composite line for piecewise linear trends) to the data. This fitted function was then subtracted from the original data. Finally, the process involved removing either the mean value or the (piecewise) linear trend from each vector or column in the data matrix to ensure a consistent baseline for further analysis. Figure 1b shows the detrended surface roughness profile of Fig. 1a.

Windowing

For the analysis of random roughness profiles, a window function is necessary to handle the finite-length data set effectively (Kay 1988). The Welch window function (Welch 1967) is particularly suitable for spectral analysis because it ensures that a windowed signal has a seamless periodic extension, which is essential for discrete Fourier transform (DFT). When the "periodic" option is specified, the function generates a window of length n + 1, returning only the first n points to achieve this periodic alignment. The Welch window, defined as a polynomial window with a single parabolic segment, is calculated as shown in Eq. 4.

$$w(k) = 1 - \left(\frac{k}{N-1}\right)^2, n = 0, 1, ..., n-1$$
 (4)

In this equation, k represents the position index of each sample in the window, ranging

from 0 to n-1, with w(k) applying a parabolic weight to each sample based on its position. This periodic window, wrapping around the cyclic interval 0, 1, ..., m-1, is specifically designed for DFT applications, where m represents the window length and must be an integer greater than 1. In the formula, N represents n/2, setting the basis for the parabolic taper.

Figure 1c illustrates the Welch-windowed surface roughness profile derived from the detrended surface roughness profile shown in Fig. 1b. To prepare nonperiodic surface roughness data for Fourier transformation, they are multiplied by a periodic window function. This windowing process in the Fourier domain effectively acts as a low-pass filter, mitigating the high-frequency noise commonly observed at terrain edges.

One-dimensional PSD

The PSD was computed to analyze the distribution of power across different spatial frequencies in the roughness profile of facial tissue products (Krim and Palasantzas 1995). The transformation from the spatial domain to the frequency domain was achieved using FFT, as expressed in Eq. 5,

$$F(k) = \sum_{n=0}^{N-1} \bar{Z}(n)w(n) \cdot e^{-\frac{i2\pi kn}{N}}, k = 0, 1, \dots, N-1$$
 (5)

where F(k) is the FFT result at the frequency index k, representing the amplitude and phase of the kth frequency component, $\bar{Z}(n)$ is the detrended roughness profile, w(n) is the Welch window function, and $e^{-\frac{i2\pi kn}{N}}$ is the complex exponential term representing the Fourier basis function for frequency k.

The PSD, P(f), for a given frequency f is mathematically defined as in Eq. 6,

$$P(f) = \frac{|F(f)|^2}{\Delta f} \tag{6}$$

where Δf is the frequency bin width, calculated as $\Delta f = \frac{1}{T}$. Here, T is the total duration of the sampled data. $|F(f)|^2$ is the squared magnitude of the FFT result, representing the power at frequency f. The resulting one-dimensional PSD (1D-PSD) plot is shown in Fig. 1d, where the log-log scale reveals frequency-dependent roughness characteristics.

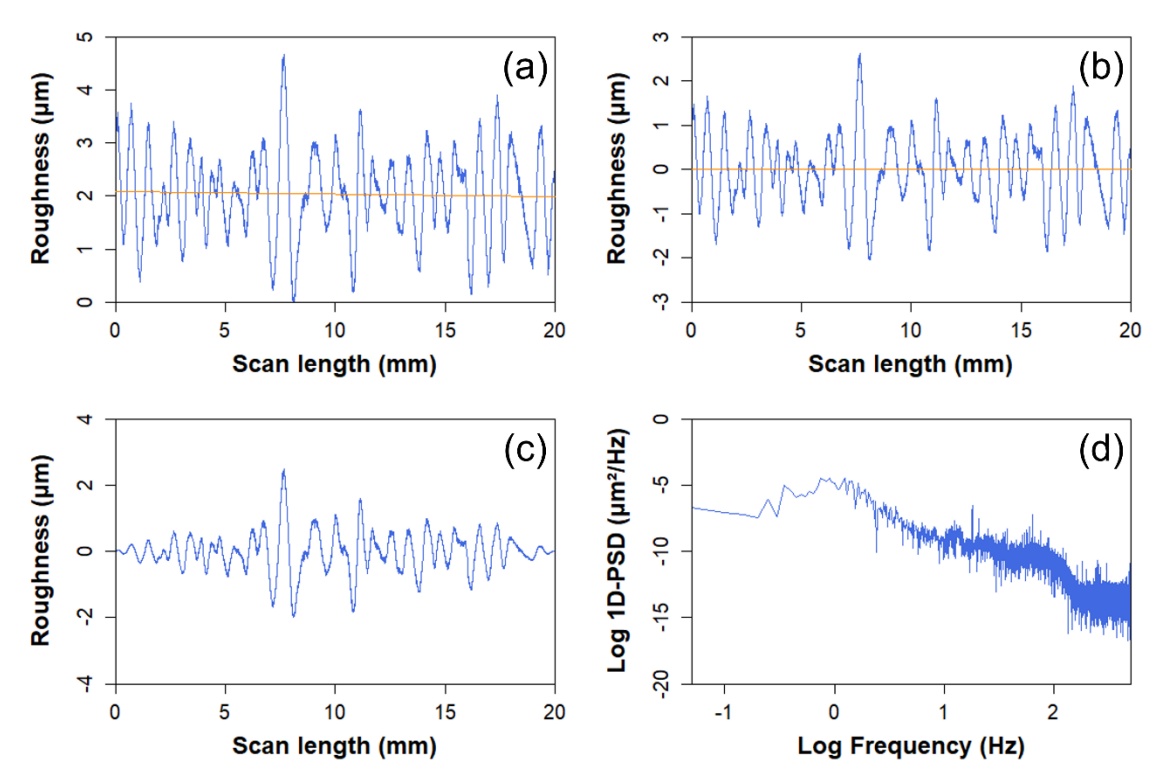


Fig. 1. Roughness profile conversion to the 1D-PSD spectrum (a, roughness profile; b, detrended roughness profile; c, Welch-windowed roughness profile; d, 1D-PSD of the roughness profile)

Principal Component Analysis of 1D-PSD spectra

Principal component analysis (PCA) was conducted to uncover hidden patterns and structures within the 1D-PSD spectra of the facial tissue. The high-dimensional 1D-PSD spectra were transformed into new orthogonal principal components (PCs), and the results were visualized in a two-dimensional space using the first two PCs.

Multilayer Perceptron for Predicting the ISV Softness of Facial Tissues *Dataset splitting*

Figure 2 shows a diagram for predicting the ISV softness of facial tissues using multilayer perceptron (MLP). For the construction of MLP models, the 1D-PSD spectra of the tissue products were utilized. The dataset was independently divided into training and test sets at a ratio of 7:3, and these subsets were used for model construction and evaluation.

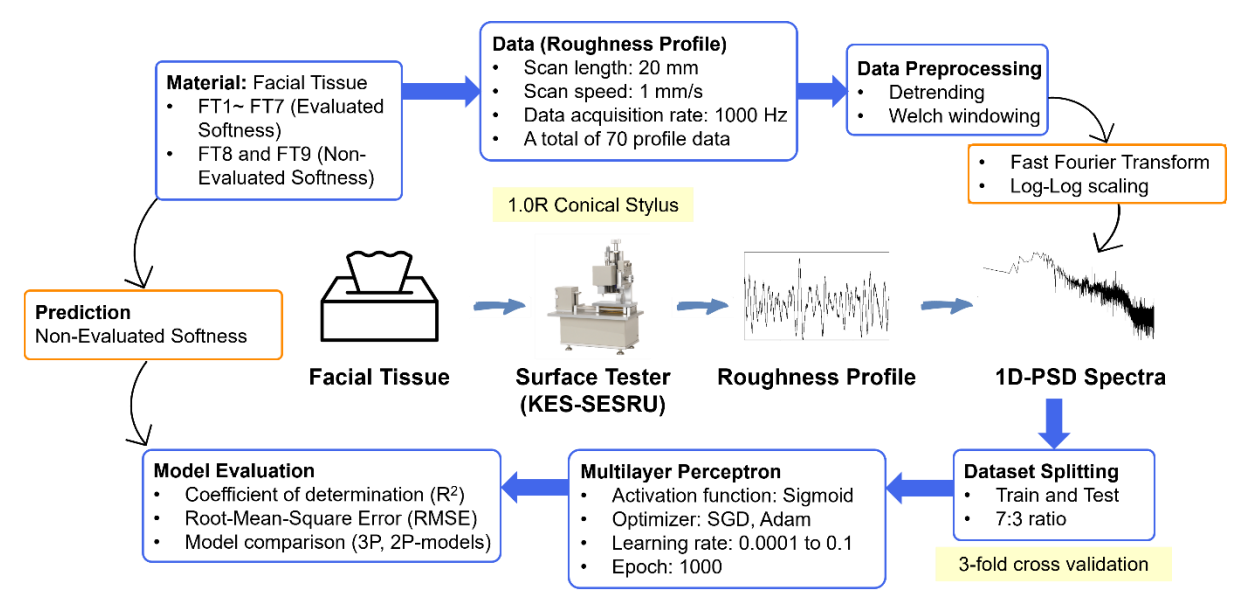


Fig. 2. Diagram for predicting the ISV softness of facial tissue products using MLP models

MLP regressors

MLP regressors were trained using backpropagation, with no activation function applied in the output layer. A sigmoid activation function was employed in the hidden layers. The squared error was used as the loss function, and the model was optimized using stochastic-gradient-descent-based optimizers, specifically SGD and Adam. Various network architectures, as detailed in Table 2, were tested with logarithmic learning rates ranging from 0.0001 to 0.1 to identify the optimal network configuration for the MLP. The maximum number of iterations was set to 1000. Hyperparameters, including the network architectures, optimizers, and learning rates, were optimized through a grid search with threefold cross-validation.

Table 2. Tested Network Architectures of MLP Regressors

Three-layer MLP				Four-layer MLP				
Input	Hidden layers Output		Input	Hidden layers		ers	Output	
layer	1st	2nd	layer	layer	1st	2nd	3rd	layer
	16	16			16	16	16	
	32	32			32	32	32	
1941	64	64	4	1941	64	64	64	4
1941	128	128	I	1941	128	128	128	
	256	256			256	256	256	
	512	512			512	512	512	

Evaluation metrics

The coefficient of determination (R²) and the root-mean-square error were used as performance metrics for the MLP models, as expressed in Eqs. 7 and 8, respectively.

$$R^2 = 1 - \frac{\sum_i (ISV_i - I\widehat{SV}_i)^2}{\sum_i (ISV_i - \mu)^2} \tag{7}$$

$$RMSE = \sqrt{\frac{1}{n} \sum_{i=1}^{n} \left(\widehat{ISV}_{i} - ISV_{i} \right)^{2}}$$
 (8)

where ISV_i and ISV_i are the analyzed and predicted ISV softness of the i^{th} observation, respectively. The parameter μ denotes the overall mean, whereas n refers to the total number of observations. All processes were performed using R software (R Core Team, ver. 4.4.1, Auckland, New Zealand), including the data preprocessing and predictive modeling of softness.

Prediction of ISV Softness for Facial Tissues

FT8 and FT9, which did not evaluate the ISV softness, were used to predict the ISV softness using the constructed MLP model. The surface roughness profiles of FT8 and FT9 were obtained using the same method as for FT1 to FT7. Subsequently, their 1D-PSD spectra were used to predict the ISV softness using the MLP model. PCA was also performed to observe the relationship between existing data and these samples (FT8 and FT9).

RESULTS AND DISCUSSION

Determination of the Surface Roughness of Facial Tissue Products

Table 3 presents the results for R_a and RMAD of the facial tissue products. In previous research (Park *et al.* 2021; Y. J. Lee *et al.* 2023), the surface profile parameter RMAD was considered to be more stable and reliable. The findings in Table 3 aligned with these observations, as RMAD and its coefficient of variation (COV) were significantly lower than those of R_a . This supports the argument that RMAD is a more accurate measure of the true surface profile as it is less influenced by testing conditions compared with R_a .

Stylus	1.0R Conical Stylus				U-Tube Stylus			
Comple	Ra (µm)		RMAD (µm)		R₄ (μm)		<i>RMAD</i> (µm)	
Sample	Avg.	COV (%)	Avg.	COV (%)	Avg.	COV (%)	Avg.	COV (%)
FT1	2.49	23.5	1.44	14.4	2.18	22.9	1.33	14.3
FT2	2.53	18.2	1.47	12.1	2.25	11.6	1.38	7.5
FT3	3.95	14.7	2.30	6.3	4.14	11.8	2.59	7.1
FT4	3.17	14.2	1.82	7.4	3.03	15.5	1.84	8.2
FT5	2.69	10.0	1.52	6.4	2.78	15.2	1.73	7.3
FT6	3.03	19.8	1.77	14.3	3.13	10.1	1.85	5.9
FT7	3.77	21.8	2.23	8.2	3.77	12.2	2.24	4.3

Table 3. Results for R_a and RMAD of Facial Tissues (Y. J. Lee *et al.* 2023)

Figure 3 compares the U-tube stylus and the 1.0R conical stylus for surface roughness characterization. The regression equations presented in the figure demonstrate a high correlation, with an R² value approaching 0.95. Notably, for *RMAD*, as shown in Fig. 3b, the slopes were greater than one, indicating that the 1.0R conical stylus detected surface structures with higher sensitivity. This difference can be attributed to the distinct contact areas of each stylus. The U-tube stylus, with a width of 0.5 mm and length of 5 mm, has a relatively large contact area with the sample surface, which may reduce its sensitivity to fine surface features. In contrast, the 1.0R conical stylus has a much smaller, approximately circular contact area, resulting in higher sensitivity to subtle surface variations. This design enhances its ability to detect subtle variations in surface roughness (Park *et al.* 2021; Moon *et al.* 2022; Lee *et al.* 2023).

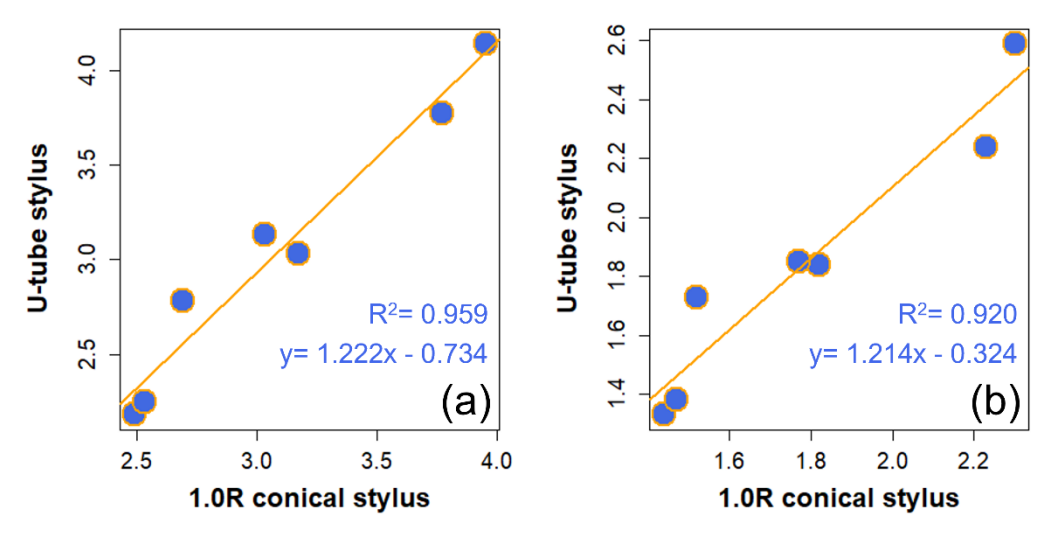


Fig. 3. U-tube stylus vs. 1.0R conical stylus for surface roughness characterization (a, R_a ; b, RMAD) of facial tissue products

1D-PSD Spectra for the Surface Roughness Profiles of Facial Tissues

Figure 4 illustrates the 1D-PSD spectra for the surface roughness profiles of the facial tissue products, whereas Table 4 provides the surface roughness contributions across different wavelength regions. The analysis revealed that most of the surface roughness contributions originated from the 100- to 1,000- μ m region, which corresponded to the medium scale, with contributions approaching almost 100%, indicating that intermediate and macroscale features such as creping and embossing dominated the surface texture. These features produce relatively shallow amplitude variations ($R_a = 2$ to 4 μ m), yet span large spatial wavelengths, resulting in a surface profile characterized by broad undulations with moderate vertical depth.

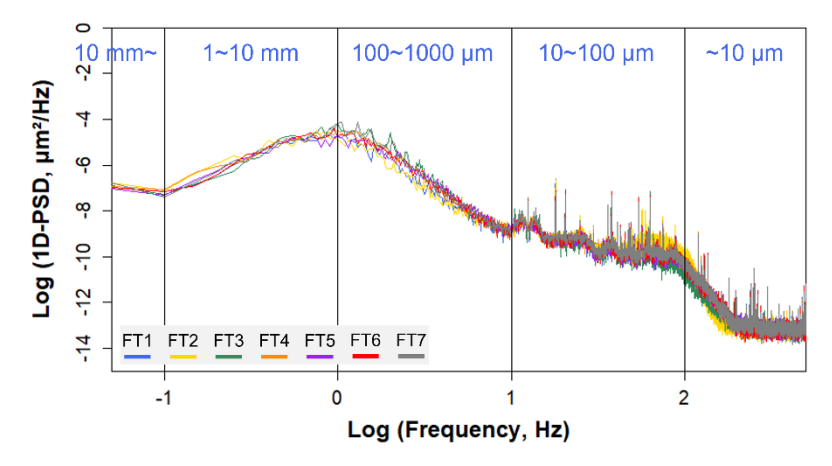


Fig. 4. 1D-PSD spectra for the surface roughness profiles of facial tissue products in the frequency domain

	Contribution of Surface Roughness, %						
Sample	1 mm≥	100 to 1,000 μm	10 to 100 μm	≤10 µm			
FT1	_	99.3	0.7	_			
FT2	_	98.5	1.5	_			
FT3		99.7	0.2	_			
FT4		99.6	0.3	_			
FT5		99.5	0.5	_			
FT6		99.6	0.4	_			
FT7	_	99.8	0.2				

Table 4. Contribution of Surface Roughness Across Different Wavelength Ranges for Facial Tissue Products

Figure 5 illustrates this concept by comparing two sinusoidal surface profiles: one with larger amplitude variations and another with smaller amplitude but higher frequency. This demonstrates that even when the average roughness is low, the actual surface profile may contain components with significant amplitude variations across different spatial scales. This phenomenon has been recently emphasized in the authors' own research (Lee *et al.* 2025). Therefore, this highlights that absolute texture parameters may not fully represent all aspects of the surface morphology.

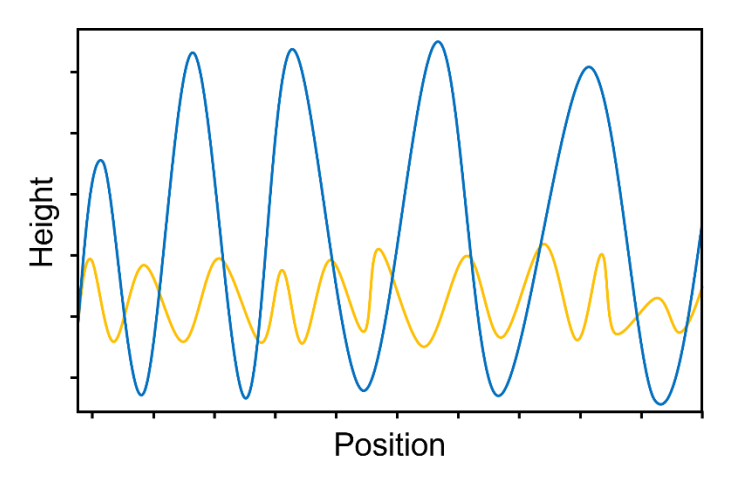


Fig. 5. Conceptual illustration of surface profiles with varying amplitude and spatial wavelength, demonstrating how broad undulations with moderate vertical depth can produce low average roughness values

Surface roughness of tissue products can be attributed to multiple sources operating at different length scales (Kajanto *et al.* 1998). At the microscale (10 to 100 μ m), free fiber ends and fiber morphology predominantly influence roughness, giving rise to high-frequency, high-resolution features. At the mesoscale (100 to 1,000 μ m), processes such as creping and small-scale printing contribute significantly, resulting in intermediate-frequency characteristics. At the macroscale (greater than 1,000 μ m), embossing, large-scale printing, and fabric patterns prevail, producing low-frequency, low-resolution surface features. Understanding these contributions from each scale is crucial for accurately characterizing and optimizing the surface properties of tissue and towel products.

In the case of facial tissue, surface roughness is primarily attributed to the medium scale, primarily reflecting the effects of the creping process. A smaller portion of the surface roughness originated from the microscale, which is associated with fiber-level morphology. Based on the data in Table 4, contributions from macroscale features

exceeding 1 mm were found to be insignificant in the surface roughness of facial tissue products. Additionally, high-frequency features below 10 μ m contributed negligibly to the characterization of surface roughness in the facial tissue products. Therefore, both macroscale features and high-frequency components smaller than 10 μ m should be excluded from the 1D-PSD analysis of facial tissue, a process referred to as applying a "cutoff" (Jacobs *et al.* 2017).

Table 5 presents the contributions of surface roughness within the wavelength range of 100 to 1,000 μm for facial tissues, further segmented into four wavelength intervals: 750 to 1,000 μm , 500 to 750 μm , 250 to 500 μm , and 100 to 250 μm . The results indicated that surface roughness primarily originated from the 750- to 1,000- μm segment, accounting for $\sim\!\!73$ to 84% of the total contribution across all samples. This finding underscores the dominant influence of larger-scale features within the medium scale on the surface roughness of the facial tissue products.

The 500- to 750- μ m interval accounted for 14.7 to 23.9% of the total surface roughness contribution, highlighting its secondary role in shaping the surface characteristics of the studied tissue products. In contrast, contributions from the 250- to 500- μ m and 100- to 250- μ m intervals were minimal, collectively contributing less than 5% across all samples. Notably, the 100- to 250- μ m interval occasionally exhibited negligible contributions, as observed in FT3.

These results further emphasized that the medium-scale roughness of facial tissue products is predominantly influenced by features in the upper range of the 100- to 1,000- µm spectrum, such as creping patterns. Smaller-scale features, although present, contributed minimally to the overall surface roughness profile. This analysis provides valuable insights into scale-specific contributions to surface roughness and supports the optimization of manufacturing processes to achieve desired surface properties.

Table 5. Surface Roughness Contribution Within the Wavelength Range of 100 to $1{,}000~\mu m$ for Facial Tissues

	Contribution of Surface Roughness (%)						
Sample	750 to 1000 μm	500 to 750 μm	250 to 500 μm	100 to 250 μm			
FT1	77.1	21.1	1.8	0.1			
FT2	78.4	18.8	2.6	0.2			
FT3	83.6	15.7	0.7				
FT4	79.6	18.6	1.6	0.2			
FT5	73.3	23.9	2.6	0.1			
FT6	79.8	18.2	1.9	0.1			
FT7	84.0	14.7	1.2	0.1			

Figure 6 shows the 1D-PSD spectra for the surface roughness profiles of facial tissues within the wavelength range of 100 to 1,000 μm . Table 6 presents the average 1D-PSD of the surface roughness profiles for the facial tissues within the wavelength range of 100 to 1,000 μm .

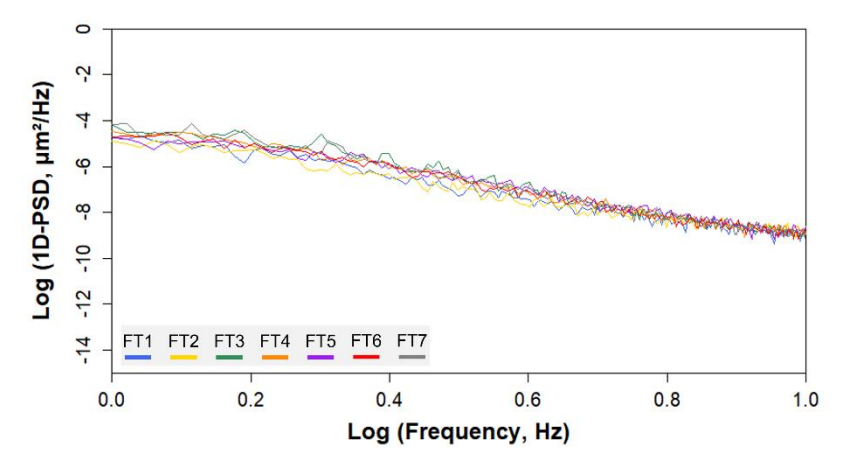


Fig. 6. 1D-PSD spectra for the surface roughness profiles of facial tissues in the frequency domain within the wavelength range of 100 to $1,000 \mu m$

Table 6. Average 1D-PSD of Surface Roughness Profiles for Facial Tissues Within the Wavelength Range of 100 to 1,000 μm

	Average 1D-PSD (μm²/Hz) in the wavelength of 10 to 100 μm							
Sample	750 to 1000 μm	500 to 750 μm	250 to 500 μm	100 to 250 μm				
FT1	-4.81	-5.13	-6.05	-6.85				
FT2	-4.76	-5.12	-5.76	-6.36				
FT3	-4.52	-5.06	-6.18	-6.83				
FT4	-4.70	-5.09	-5.90	-6.31				
FT5	-4.90	-5.18	-5.91	-6.66				
FT6	−4.70	−5.12	-5.97	-6.88				
FT7	-4.66	-5.13	-5.98	-6.72				

Figure 7 illustrates the correlation between the normalized (min-max normalization) average 1D-PSD and the surface roughness metrics, with Fig. 7a representing R_a and Fig. 7b representing RAD. There was a significant correlation between the 1D-PSD values in the wavelength range of 750 to 1000 μ m and the surface roughness parameters, with R^2 values of 0.659 for R_a and 0.737 for RMAD. These findings indicated that the surface roughness characteristics in this range were predominantly influenced by medium-scale features, such as creping effects, which played a key role in defining the roughness profile of the facial tissue products.

Furthermore, the slightly higher correlation between 1D-PSD and RMAD compared with that with R_a suggests that RMAD is a more accurate measure of the true surface profile, as discussed previously. This reinforces the utility of RMAD as a reliable parameter for surface roughness characterization.

In contrast, the contributions from other wavelength ranges, such as 500 to 750 μm , 250 to 500 μm , and 100 to 250 μm , showed weaker correlations with the roughness metrics. This suggests that the fine-scale features within these regions do not significantly influence the overall roughness.

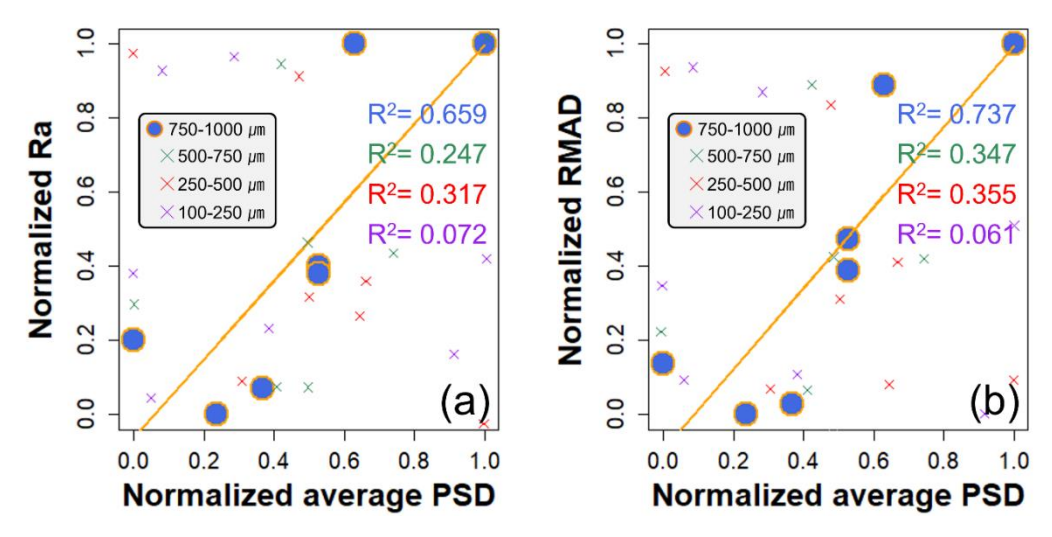


Fig. 7. Correlation between the normalized average 1D-PSD and surface roughness metrics: (a) *Ra* and (b) *RMAD*

PCA of 1D-PSD Spectra

Figure 8 shows the PCA score plots of the first two PCs in the wavelength range of 10 to 1,000 μ m (Fig. 8a) and 100 to 1,000 μ m (Fig. 8b). The PCA score plots in Fig. 8 insightfully visualize the 1D-PSD spectra. Although the surface roughness contributions were primarily observed in the wavelength range of 100 to 1,000 μ m, as previously analyzed, the PCA results revealed an interesting phenomenon: when the full wavelength range (10 to 1,000 μ m) was considered, better clustering characteristics among the samples were observed.

This discrepancy suggests that although roughness contributions primarily originate from medium-scale features (100 to 1,000 μ m), the inclusion of microscale features (10 to 100 μ m) in the PCA analysis provides subtle differences that enhance the separation and clustering of the samples in the multidimensional space. This finding implies that microscale features, although contributing minimally to the overall roughness, may carry unique information that aids in distinguishing samples more effectively.

In practical terms, it is beneficial to consider a broader wavelength range in machine learning model construction, even when the primary contribution is localized to a specific region, such as 100 to $1{,}000$ μm .

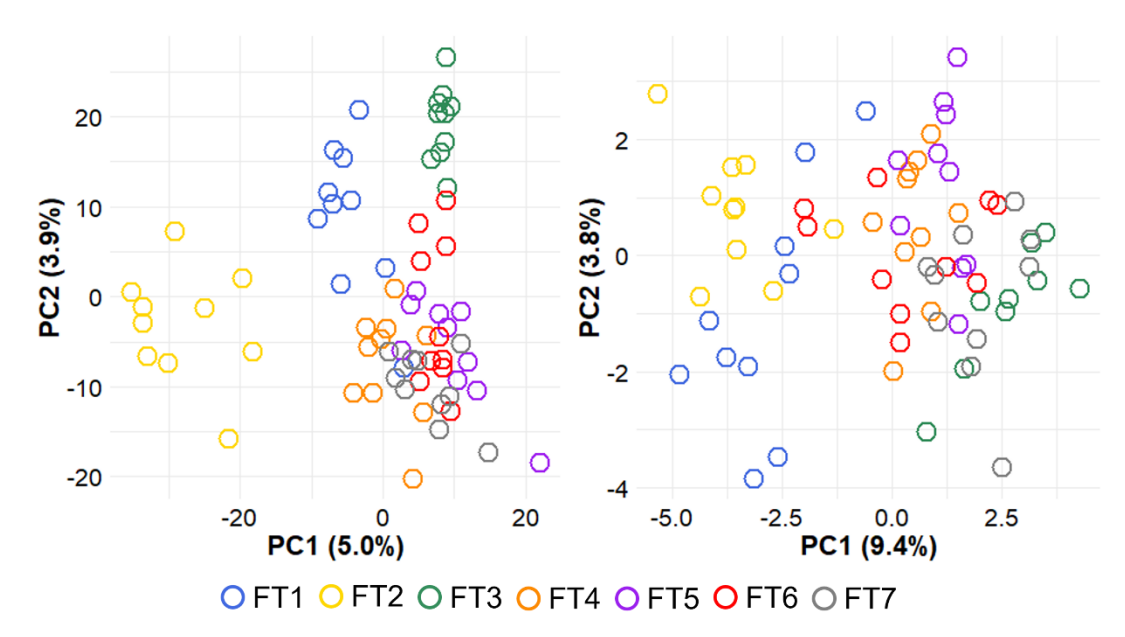


Fig. 8. PCA score plots of the first two PCs in the wavelength range of 10 to 1,000 μ m (a) and 100 to 1,000 μ m (b)

MLP for Predicting the Softness of Facial Tissues

As discussed in the PCA results, the 1D-PSD spectra in the wavelength range of 10 to 1,000 μ m were used in the MLP regression model to predict the ISV softness of facial tissues. Although the primary roughness contribution originated from medium-scale features (100 to 1,000 μ m), the inclusion of microscale features (10 to 100 μ m) introduced subtle differences that enhanced sample differentiation in complex tasks.

Figure 9 illustrates the optimized MLP architecture for predicting the ISV softness of facial tissues, which was determined through a grid search. The 1D-PSD spectra in the wavelength range of 10 to $1,000~\mu m$ comprised 1,981 input variables. The finalized model consisted of three hidden layers, each employing a sigmoid activation function, with each hidden layer containing 16 nodes. The SGD optimizer was selected, and the optimal learning rate was set to 0.1.

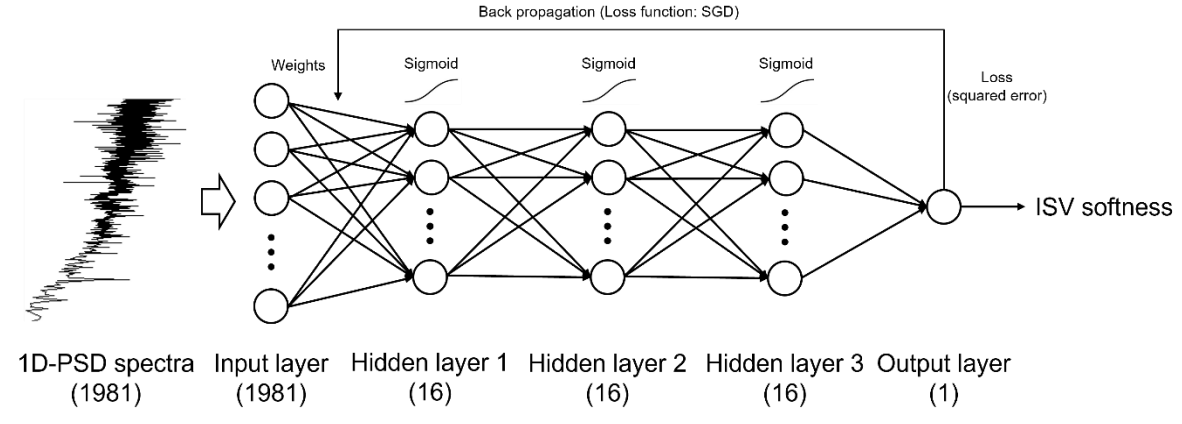


Fig. 9. Architecture of the MLP for predicting the ISV softness of facial tissues

Figure 10 shows the predicted ISV softness using three models: the MLP model trained with 1D-PSD spectra (a), the 3-P model incorporating *TM*, *RMAD*, and surface friction (b), and the 2-P model utilizing *TM* and *RMAD* (c). The results indicated that the MLP model significantly outperformed both the 3-P and 2-P models, as evidenced by its higher R² value (0.860). This superior performance was achieved solely using the roughness profile data derived from 1D-PSD spectra without requiring additional measurements of *TM* and surface friction. These findings highlight the efficiency and practicality of the MLP model as it eliminates the need for labor-intensive and time-consuming measurements, offering an effective approach for predicting the softness of facial tissues.

However, the R² value of the MLP model did not reach a perfect 1.0, which may be attributed to the absence of friction data and *TM* in the model. These parameters, being integral components of surface and bulk softness, could have provided additional explanatory power for capturing variations in ISV softness. Consequently, although the MLP model demonstrated strong predictive capabilities, the inclusion of these missing variables might further enhance its performance.

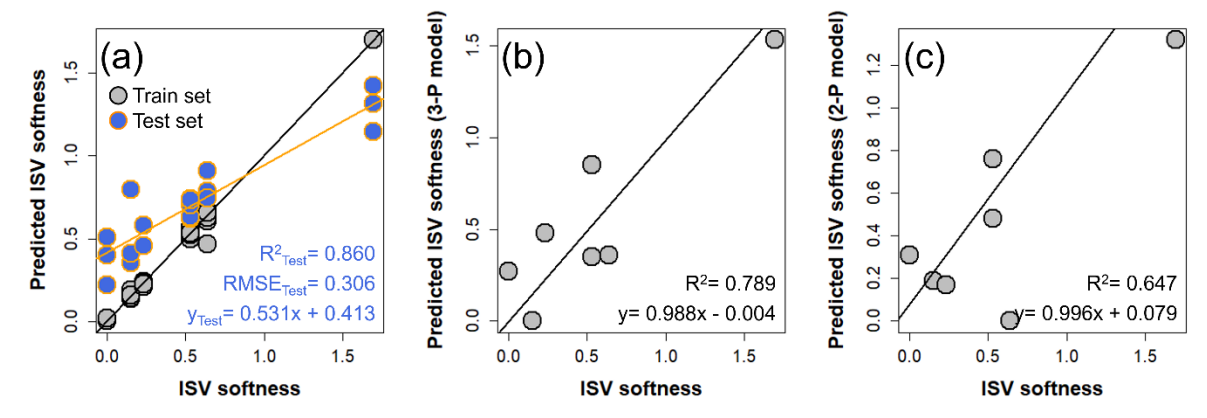


Fig. 10. Predicted ISV softness from the MLP (a), 3-P (*TM*, *RMAD*, and surface friction) (b), and 2-P (*TM*, and *RMAD*) (c) models (Lee *et al.* 2023)

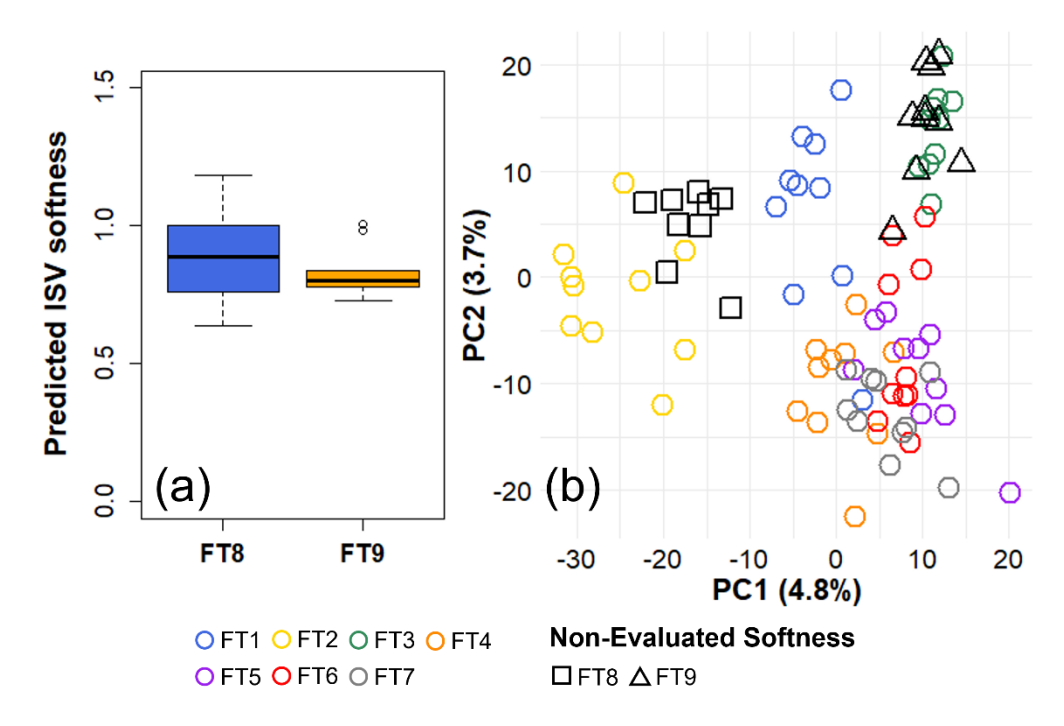


Fig. 11. Predicted ISV softness for FT8 and FT9 (a) and their placement on a PC score plot alongside existing facial tissue products (b)

Prediction of ISV Softness for Facial Tissues

The established MLP model was utilized to predict the ISV softness of FT8 and FT9, whose softness values had not been previously evaluated. Figure 11a presents the box plots of the predicted ISV softness for these samples.

For FT8, the box plot shows a median ISV softness of \sim 0.90, with most predicted values ranging between 0.6 and 1.2, indicating some variability in the predictions. In contrast, FT9 displays a narrower range of predicted ISV softness, with a median value close to 0.80. The interquartile range is small, suggesting consistent predictions for this sample, although two significant outliers are observed.

Figure 11b illustrates the placement of FT8 and FT9, whose ISV softness values were not evaluated, on a PC score plot alongside existing facial tissue products (FT1 to FT7).

Technical Significance

The proposed approach achieved satisfactory performance in predicting softness values obtained from established pair-comparison tests, without directly relying on sensory panel testing (SPT), which requires a trained panel and is both time-consuming and resource-intensive. Although tensile modulus (TM) and surface friction measurements were not included in this study, the method demonstrated promising predictive capability. Future studies will focus on investigating the fractal surface characteristics of tissue products using PSD techniques, which can provide additional insights into surface complexity and autocorrelation beyond conventional surface parameters.

CONCLUSIONS

- 1. The 1.0R conical stylus was successfully applied to obtain surface roughness profiles, showing a high correlation with the U-tube stylus. Additionally, the 1.0R conical stylus proved suitable for acquiring the 1D-PSD spectra of facial tissues given its minimal contact area.
- 2. The 1D-PSD spectra revealed the contributions of surface roughness for facial tissues across different wavelength ranges. The 100- to 1,000-µm range was identified as the dominant contributor, attributed to the medium-scale roughness primarily influenced by creping effects.
- 3. The ISV softness represents a linear and continuous measure of subjective softness, derived via a pair-comparison testing method known as the Ko-method, ensuring objective quantification of tactile perceptions. The MLP model for predicting the ISV softness of facial tissues was established and trained using 1D-PSD spectra in the range of 10 to 1,000 μm. Although the high-contribution range was primarily 100 to 1,000 μm, the inclusion of the 10- to 100-μm range introduced subtle differences that enhanced the sample separation and clustering in multidimensional space.
- 4. The MLP model demonstrated high predictive performance for the ISV softness of facial tissue products using 1D-PSD spectra, achieving an *R*² value of 0.860 on the test dataset. This model outperformed previously developed models (3-P and 2-P models), highlighting its efficiency and practicality.

ACKNOWLEDGMENTS

The authors would like to acknowledge the financial support provided by the Ministry of Science and ICT (Information and Communication Technology) of the Korean government and the National Research Foundation of Korea (Grant No. RS-2023-00301889).

REFERENCES CITED

- Aguilar, J. R., Arenas, J. P., and Salinas, R. (2009). "Friction noise technique for the measurement of surface roughness of papers," *Applied Acoustics* 70(9), 1235-1240. DOI: 10.1016/j.apacoust.2009.03.008
- Ampulski, R. S., Sawdai, A. H., Spendel, W., and Weinstein, B. (1991). "Methods for the measurement of the mechanical properties of tissue paper," in: *Proceedings of the International Paper Physics Conference*, Kona, HI, USA.
- Beuther, P. D., Ko, Y., Pawar, P., Raynor, W. J., Rekoske, M. J., and Ries, T. D. (2012). "Molded wet-pressed tissue," U. S. Patent No. US8257551B2, Kimberly ClarkWorldwide, Inc.
- Blackman, R. B., and Tukey, J. (1959). *The Measurement of Power Spectra: From the Point of View of Communications Engineering*, Dover Publications, Mineola, NY, USA.
- Boidi, G., Da Silva, M. R., Profito, F. J., and Machado, I. F. M. (2020). "Using machine learning radial basis function (RBF) method for predicting lubricated friction on

- textured and porous surfaces," *Surface Topography: Metrology and Properties* 8(4), article 044002. DOI: 10.1088/2051-672X/abae13
- Borchers, H. (2022). "Pracma: Practical numerical math functions (2.4. 2)," (https://cran.r-project.org/web/packages/pracma/pracma.pdf), Accessed December 16, 2024.
- Hasan, B., and Karabacak, Y. E. (2023). "Triboinformatic modeling of the friction force and friction coefficient in a cam-follower contact using machine learning algorithms," *Tribology International* 181, 108336. DOI: 10.1016/j.triboint.2023.108336
- Hollmark, H. (1983). "Evaluation of tissue softness," Tappi Journal 66(2), 97-99.
- Hollmark, H., and Ampulski, R. S. (2004). "Measurement of tissue paper softness: A literature review," *Nordic Pulp and Paper Research Journal* 19(3), 345-353. DOI: 10.3183/npprj-2004-19-03-p345-353
- Hwang, S.-W., Park, G., Kim, J., Kang, K.-H., and Lee, W.-H. J. B. (2024). "One-dimensional convolutional neural networks with infrared spectroscopy for classifying the origin of printing paper," *BioResources* 19(1), 1633-1651. DOI: 10.15376/biores.19.1.1633-1651
- Jacobs, T. D. B., Junge, T., and Pastewka, L. (2017). "Quantitative characterization of surface topography using spectral analysis," *Surface Topography: Metrology and Properties* 5(1). DOI: 10.1088/2051-672X/aa51f8
- Kajanto, I., Laamanen, J., and Kainulainen, M. (1998). "Paper bulk and surface," in: *Paper Physics*, K. Niskanen (ed.), Fapet Oy, Jyväskylä, Finland.
- Kay, S. M. (1988). Modern Spectral Estimation, Pearson Education India, Chennai.
- Kim, K.-J., Kim, J.-H., Park, G., and Jeong, M.-J. (2023). "Predictive modeling of Korean traditional paper characteristics using machine learning approaches (Part 2): Prediction of carbonyl content and analysis of variable importance using random forest. *Journal of Korea Technical Association of the Pulp and Paper Industry* 55(5), 13-23.
- Ko, Y. C., Park, J. Y., Lee, J. H., and Kim, H. J. (2017). "Principles of developing a softness evaluation technology for hygiene paper," *Journal of Korea Technical Association of The Pulp and Paper Industry* 49(4), 184-193. DOI: 10.7584/iktappi.2017.08.49.4.184
- Ko, Y. C., Park, J. Y., Melani, L., Park, N. Y., and Kim, H. J. (2018). "Principles of developing physical test methods for disposable consumer products," *Nordic Pulp and Paper Research Journal* 34(1), 75-87. DOI: 10.1515/npprj-2018-0029
- Ko, Y. C., and Park, J.-M. (2016). "Developing objective linear scale data from subjective tests for consumer products," *Journal of Korea Technical Association of the Pulp and Paper Industry* 48(1), 19-26. DOI: 10.7584/ktappi.2016.48.1.019
- Ko, Y. C., Park, J.-M., and Moon, B.-G. (2015). "Development of an objective softness evaluation method and its standardization for hygiene paper," *Journal of Korea Technical Association of The Pulp and Paper Industry* 47(5), 80-84. DOI: 10.7584/ktappi.2015.47.5.080
- Krim, J., and Palasantzas, G. J. (1995). "Experimental observations of self-affine scaling and kinetic roughening at sub-micron lengthscales," *International Journal of Modern Physics B* 9(6), 599-632.
- Kweon, S. W., Ko, Y. C., Lee, Y. J., Cha, J. E., Moon, B. G., and Kim, H. J. (2024). "Determination of in-use properties of paper towels," *BioResources* 19(4), 7366-7380. DOI: 10.15376/biores.19.4.7366-7380
- Lee, J. H., Park, J. Y., Kim, H. J., and Ko, Y. C. (2017). "A new subjective softness

- evaluation method for hygiene paper," *Journal of Korea Technical Association of The Pulp and Paper Industry* 49(4), 178-183. DOI: 10.7584/jktappi.2017.08.49.4.178
- Lee, J. M., Ko, Y. C., Moon, B. G., Lee, Y. J., Kweon, S. W., and Kim, H. J. (2023). "Developing physical softness models for facial tissue products," *BioResources* 19(1), 116-133. DOI: 10.15376/biores.19.1.116-133
- Lee, Y. J., Kim, G. W., Lee, T. J., and Kim, H. J. (2025). "Fractal geometry: Surface characterization of printing paper," *Fractal and Fractional* 9(2), article 123. DOI: 10.3390/fractalfract9020123
- Lee, Y. J., Ko, Y. C., Moon, B. G., and Kim, H. J. (2023). "Surface characterization of paper products by profilometry with a fractal dimension analysis," *BioResources* 18(2), 3978-3994. DOI: 10.15376/biores.18.2.3978-3994
- Moon, B. G., Park, N. Y., Ko, Y. C., and Kim, H. J. (2022). "Characterization of paper surfaces by friction profilometry," *BioResources* 17(4), 6067-6078. DOI: 10.15376/biores.17.4.6067-6078
- Motamedi, N., Magnier, V., and Wannous, H. J. (2023). "Towards the identification of the link between the contact roughness and the friction-induced vibration: Use of deep learning," *European Journal of Mechanics A/Solids* 99, article 104949.
- Park, N. Y., Ko, Y. C., Kim, H. J., and Moon, B. G. (2021). "Surface characterization of paper products via a stylus-type contact method," *BioResources* 16(3), 5667-5678. DOI: 10.15376/biores.16.3.5667-5678
- Pawlak, J. J., Frazier, R., Vera, R. E., Wang, Y., and Gonzalez, R. (2022). "The softness of hygiene tissue," *BioResources* 17(2), 3509-3550. DOI: 10.15376/biores.17.2.Pawlak
- Ramasubramanian, M. (2001). "Physical and mechanical properties of towel and tissue," in: *Handbook of Physical Testing of Paper*, CRC Press, Boca Raton, FL, USA, pp. 683-896.
- Thurstone, L. L. (1994). "A law of comparative judgment," *Psychological Review* 101(2), 266.
- Welch, P. J. (1967). "The use of fast Fourier transform for the estimation of power spectra: A method based on time averaging over short, modified periodograms," *IEEE Transactions on Audio and Electroacoustics* 15(2), 70-73. DOI: 10.1109/TAU.1967.1161901
- Wu, J.-J. (2000). "Spectral analysis for the effects of stylus tip curvature on measuring fractal profiles," *Measurement Science and Technology* 11(9), 1369. DOI: 10.1088/0957-0233/11/9/317

Article submitted: December 9, 2024; Peer review completed: February 1, 2025; Revised version received: June 14, 2025; Further revised version received and accepted: June 15, 2025; Published: June 23, 2025.

DOI: 10.15376/biores.20.3.6457-6475